Hindawi
International Journal of Rotating Machinery
Volume 2021, Article ID 6691574, 9 pages
https://doi.org/10.1155/2021/6691574

Research Article

Optimization Analysis of Automotive Asymmetric Magnetic Pole Permanent Magnet Motor by Taguchi Method

Wenchao Zhang, Liwei Shi, Kaiwen Liu, Lintao Li, and Jianning Jing

School of Transportation and Vehicle Engineering, Shandong University of Technology, Zibo 255049, China

Correspondence should be addressed to Liwei Shi; shiliwei@sdut.edu.cn

Received 20 November 2020; Revised 13 March 2021; Accepted 8 April 2021; Published 17 April 2021

Academic Editor: Ashwani K. Gupta

In order to improve the air-gap flux density of the permanent magnet synchronous motor and reduce the cogging torque, a novel structure with asymmetric magnetic poles for automobile was proposed. Based on the characteristics of the parallel magnetic circuit, the magnetic flux path diagram is established. And the equivalent magnetic circuit model is established by the equivalent magnetic circuit method. The Taguchi method is used to be a multiobjective optimization algorithm. The total harmonic distortion of the air-gap flux density is the first optimization goal. The second and third optimization goals are the cogging torque and the average of output torque, respectively. And the torque ripple is a constraint condition. The optimized parameter combination is obtained by the Taguchi method. Finite element simulation analysis and prototype test are carried out for the optimized motor structure. The results show that the total harmonic distortion of air-gap flux density is reduced by 36.7% comparing with the initial structure. The cogging torque is reduced by 26.0%. And the average output torque is increased by 4.8%.

1. Introduction

Electric automobile has been widely concerned around the world because of the superiority of energy saving and environmental protection. As one of the core technologies of electric automobiles, the driving motor system has become the key component. High power density, high efficiency, and wide speed range have become current research directions. At present, driving motors of electric automotive include induction motor, direct current motor, and permanent magnet synchronous motor (PMSM). PMSM has become the most promising drive motor due to its advantages of high power density, high efficiency, and simple structure [1, 2].

According to the relative position of the permanent magnet and the rotor core, PMSM can be divided into surface mount type and interior type. The interior type can be divided into three types: radial type, tangential type, and hybrid type. Their magnetization directions of the permanent magnets are different. At present, the interior PMSM is used widely in industrial engineering. Many automotive companies such as Daimler, Toyota, and BYD have widely applied interior PMSM to their electric automobile [3, 4].

However, the air-gap flux density waveform of PMSM is similar to a square wave. It has many higher harmonics. And high cogging torque is not conducive to the output performance [5].

In view of above disadvantages, domestic and foreign scholars carried out studies on the influence of output performance and different magnetic pole shapes. It is determined that the air-gap flux density and the cogging torque are greatly affected by the shape of the magnetic poles. Appropriate magnetic pole shape can improve the air-gap flux density and reduce cogging torque [6, 7]. Toyota adopted an interior PMSM structure of V-type and tangential type on Prius hybrid automobile. Oak Ridge National Laboratory proposed a U-type motor structure. The air-gap flux density is improved, and the cogging torque is reduced. But the amount of permanent magnets is increased [8]. Biasing the magnetic poles and changing the pole arc coefficient can also improve the motor performance [9–11]. In [12], the outer edge of the magnet of the surface mount PMSM was cut to improve air-gap magnetic field. But it makes the manufactural process more difficult. And it can cause sudden changes in magnetic field. For optimization methods, domestic scholars proposed

the Taguchi method for multiobjective optimization [13, 14]. It can reduce the number of experiments and improve efficiency. But the traditional Taguchi method has the same number of level values. It is difficult to obtain the best optimized solution. And the optimal motor structure cannot be obtained.

In order to improve the air-gap flux density and the cogging torque, this paper proposes a PMSM structure with asymmetric magnetic poles. The equivalent magnetic circuit model is established. And the effective magnetic flux is analyzed by the equivalent magnetic circuit method. The rotor structure is improved. Optimization goals are selected. Some key parameters are selected to be optimization variables. Using the Taguchi method, a multiobjective optimization scheme is proposed. And a two-dimensional finite element method and prototype experiment are used to verify.

2. Motor Structure and Magnetic Circuit Analysis

2.1. Motor Structure. This paper proposes PMSM structure asymmetric magnetic poles. Its three-dimensional structure is shown in Figure 1. It is an interior-type PMSM with 8 poles and 12 slots. Its winding is concentrated winding. Each of its magnetic poles is a single-layer arrangement. The shape of magnetic poles is similar with "λ." Each magnetic pole is combined with two pieces of rare earth permanent magnet materials. The thickness and length of them are different. The relevant structure parameters are shown in Table 1.

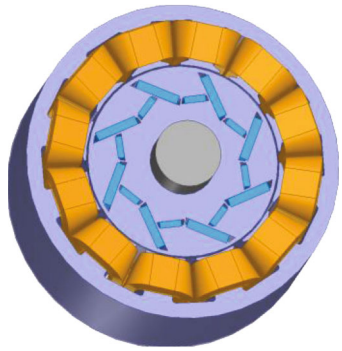

Figure 1: PMSM structure of asymmetric poles.

Table 1: Motor structure parameters.

Parameters	Value
Outer diameter of stator (mm)	145
Inner diameter of stator (mm)	89.5
Outer diameter of rotor (mm)	88
Inner diameter of rotor (mm)	30.5
Axial length (mm)	120.3
Permanent magnet material	N35SH
Silicon steel sheet grade	DW310-35
Pole slot matching	8/12

2.2. Motor Effective Flux Analysis. This paper takes a traditional V-type structure as comparing structure. Each pole effective magnetic flux of two motor structures is analyzed. Figure 2 shows the comparison diagrams of the flux paths. It can be seen that the effective flux of the traditional V-type structure is a single path. It is provided by two adjacent permanent magnets. The effective flux of asymmetric magnetic pole structure consists of two paths in parallel. A path is provided by a single long permanent magnet. And another path is provided by two adjacent permanent magnets.

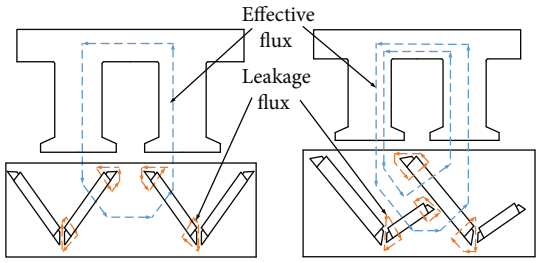

Figure 2: Comparison diagrams of flux paths.

Schematic diagrams of flux paths have been shown above. The equivalent magnetic circuit models of two motor structures are established, respectively, by the equivalent magnetic circuit method. And they are shown in Figure 3.

In Figure 3, F_L and F_S are the magnetomotive force. They are, respectively, provided by the long permanent magnet and the short permanent magnet. F_d is the direct axis component of the armature reaction. G_{mL} and G_{mS} are the internal equivalent permeance of the long permanent magnet and the short permanent magnet, respectively. $2G_{m\delta 1}$ is the permeance between the long permanent magnet and the rotor core. $2G_{m\delta 2}$ is the permeance between the short permanent magnet and the rotor core. $2G_{ll}$ is the leakage permeance of long permanent magnet. And $2G_{ls}$ is the leakage permeance of short permanent magnet. G_g is the air-gap permeance. G_T is the permeance of stator teeth. G_Y is the permeance of the stator yoke. G_{r1} is the permeance of the rotor core between long permanent magnet and the air gap. And G_{r2} is the performance of the rotor core between short permanent magnet and the air gap. G_{rp} is the permeance of the rotor core between the long and short permanent magnets. Φ_m is the total magnetic flux in a magnetic circuit. It is provided by the long and short permanent magnet. Φ_{me} is the effective magnetic flux. Φ_{ll} and Φ_{sl} are the leakage flux of long permanent magnet and short permanent magnet, respectively.

In Figure 3(b), Φ_{m1} is an extra magnetic flux in the equivalent magnetic circuit model. And it only appears in an asymmetric magnetic pole structure. G_{r1} and G_{r2} are connected in parallel. G' is used to represent the total permeance of G_{r2}, G_{rp}, $2G_{m\delta 2}$, G_{mS}, and $2G_{ls}$.

According to the superposition principle, G' meets the following conditions:

$$\frac{1}{G'} = \frac{1}{G_{r2}} + \frac{1}{G_{rp}} + \frac{(2/G_{ls}) \times ((1/G_{mS}) + (2/G_{m\delta 2}))}{(2/G_{ls}) + (1/G_{mS}) + (2/G_{m\delta 2})}. \quad (1)$$

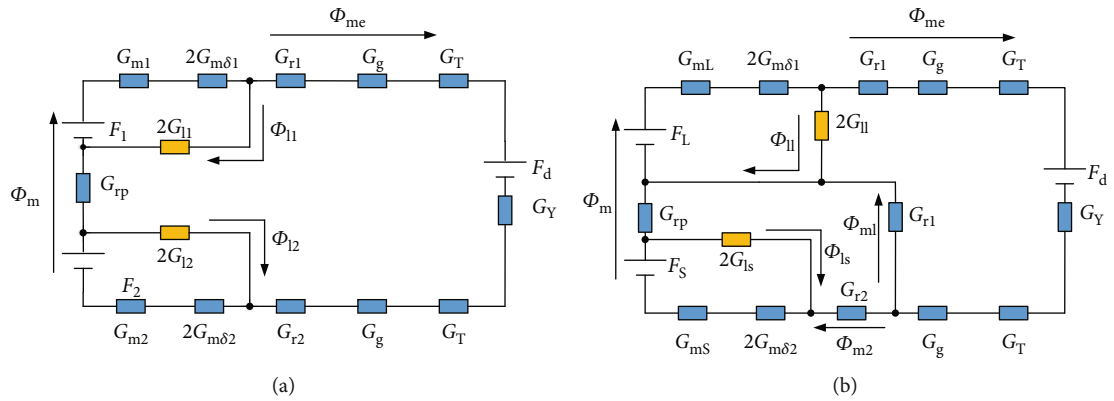

Figure 3: The equivalent magnetic circuit models: (a) traditional V-type; (b) asymmetrical magnetic poles.

G_e is used to represent the total permeance of G_{r1} and G'. It meets the following conditions:

$$\frac{1}{G_e} < \min\left\{\frac{1}{G_{r1}}, \frac{1}{G'}\right\}. \tag{2}$$

Above all, the structure with asymmetric magnetic poles can reduce the total permeance in the magnetic circuit. Its total effective magnetic flux is more than a traditional V-type structure if the magnetomotive force is the same.

3. Motor Structure Optimization

In order to obtain a better geometric motor shape, this paper makes some improvements on the rotor structure. The shape of rotor edge is changed. The auxiliary slots are used inside the rotor. The length of the air gap becomes nonuniform. The parameters are optimized by an appropriate optimization method. And the performance of the rated operating point is selected for research and analysis.

3.1. Optimization Ideas and Optimization Methods. The method of changing the air-gap length is used in this paper. The air-gap length becomes nonuniform. And the effective magnetic flux direction is adjusted. The specific measures are as follows. The auxiliary slots are used inside the rotor. It can enhance the magnetization ability and reduce the rotational inertia. The distance between auxiliary slots and a permanent magnet is d. The outer edge of the rotor is changed to be eccentric. The eccentric distance is h. Straight line is used in the junction of the eccentric circle. Its length is l. It can eliminate sharp corners on the outer edge, as shown in Figure 4.

The above improvement method can improve the air-gap flux density waveform. The schematic diagram of the expected waveform can be represented in Figure 5. It is more sinusoidal than the initial structure.

This paper uses the Taguchi method to optimize the parameters. The Taguchi method was first proposed by Dr. Genichi Taguchi who is a Japanese quality control expert. It is a local optimization method based on orthogonal experiments. It can quickly determine the combination of multiob-

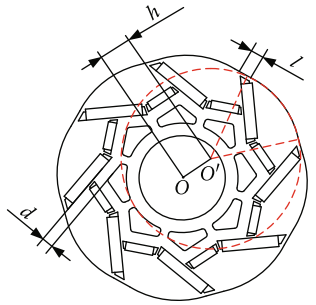

Figure 4: Rotor structure optimization.

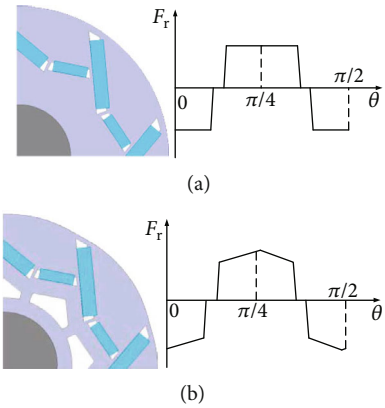

Figure 5: Schematic diagrams of the air-gap magnetic density waveform: (a) initial structure and waveform; (b) improved structure and expected waveform.

Table 2: Motor optimization parameters and level values.

Level	A (mm)	B (mm)	C (mm)
1	2	6	None
2	4	6.5	4
3	6	4	4.5
4	8	\	\
5	10	\	\
6	12	\	\

Table 3: Nonstandard orthogonal experimental matrix.

Experiment number	A	B	C
1	1	1	1
2	2	1	2
3	3	1	3
4	4	1	2
5	5	1	3
6	6	1	1
7	1	2	3
8	2	2	1
9	3	2	2
10	4	2	1
11	5	2	2
12	6	2	3
13	1	3	2
14	2	3	3
15	3	3	1
16	4	3	3
17	5	3	1
18	6	3	2

Table 4: Orthogonal experimental results.

Experiment number	THD (%)	T_{cog} (mN•m)	T_{avg} (N•m)
1	40.35	298.86	13.32
2	37.93	294.42	13.57
3	37.25	286.83	13.58
4	33.91	277.12	13.60
5	35.86	280.57	13.59
6	38.68	284.29	13.46
7	40.23	297.56	13.32
8	36.95	286.89	13.54
9	37.06	281.55	13.57
10	31.01	274.46	13.78
11	35.67	277.92	13.65
12	37.47	282.65	13.61
13	40.62	364.42	13.45
14	38.27	324.96	13.56
15	37.72	314.61	13.56
16	34.95	297.53	13.71
17	36.82	304.35	13.69
18	37.73	302.57	13.61

jective optimization with the least number of experiments. The basic design process is as follows:

(1) Determine optimization goals according to requirements

(2) Determine optimization variables and corresponding level values

(3) Establish an orthogonal experimental matrix

Table 5: The overall average value of experimental results.

	THD (%)	T_{cog} (mN•m)	T_{avg} (N•m)
Average value	37.734	302.570	13.606

Table 6: The average value of THD.

Level	A	B	C
1	40.40	36.33	36.92
2	37.72	36.40	36.15
3	37.34	37.68	36.34
4	33.29	\	\
5	36.11	\	\
6	37.96	\	\

Table 7: The average value of T_{cog}.

Level	A	B	C
1	320.28	287.02	294.02
2	302.09	283.51	295.67
3	294.33	318.07	293.91
4	283.04	\	\
5	287.61	\	\
6	289.84	\	\

Table 8: The average value of T_{avg}.

Level	A	B	C
1	13.36	13.52	13.56
2	13.56	13.60	13.57
3	13.57	13.68	13.65
4	13.70	\	\
5	13.64	\	\
6	13.56	\	\

(4) Use the finite element method to solve the orthogonal experiment matrix

(5) Analyze the influence of each optimization variable and determine the optimal parameters

(6) Verify the optimization results by finite element analysis

3.2. Determination of Optimization Goals and Optimization Variables. In this paper, the Taguchi method is used to optimize the air-gap flux density waveform, the cogging torque, and the output torque. And it must ensure that the torque ripple does not increase. Therefore, the total harmonic distortion of the air-gap flux density (THD) is the first optimization goal. The cogging torque (T_{cog}) is the second optimization goal. The average of output torque (T_{avg}) is the third optimization goal. And the torque ripple is a constraint condition. It requires that THD and T_{cog} reduces

Table 9: The proportions of the influence of each optimization variable on the optimization goal.

Optimization variables	THD		T_{cog}		T_{avg}	
	SS	Proportion	SS	Proportion	SS ($\times 10^{-3}$)	Proportion
A	4.95	82.66%	265.53	46.48%	12.78	73.17%
B	0.65	10.89%	281.93	49.35%	2.84	16.28%
C	0.39	6.45%	23.83	4.17%	1.84	10.55%
Total	5.99	100%	571.28	100%	17.46	100%

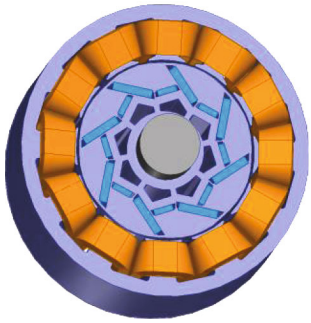

Figure 6: Motor structure after optimization.

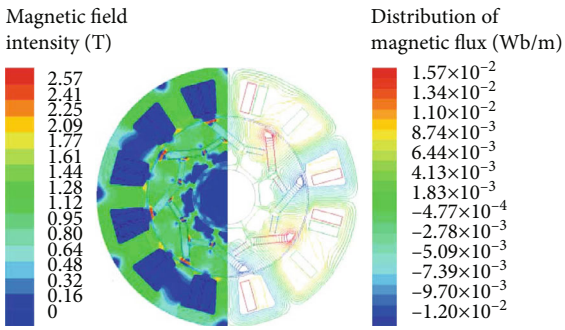

Figure 7: Static magnetic field analysis.

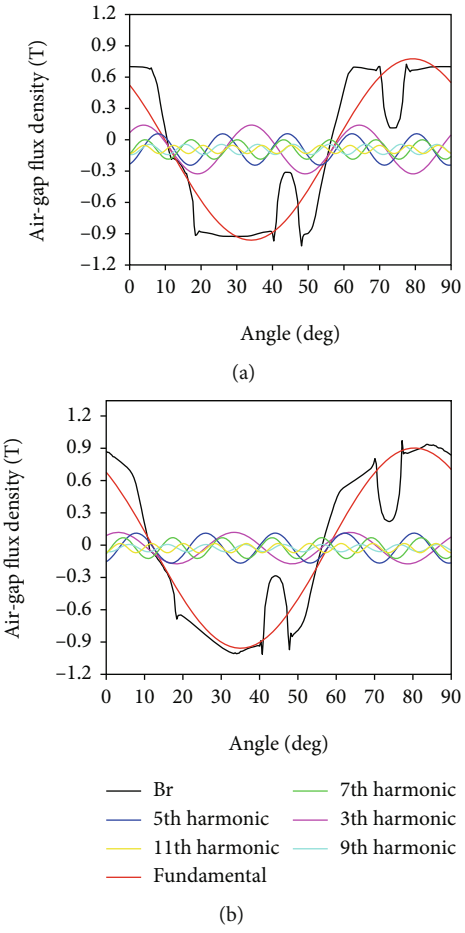

Figure 8: Air-gap flux density waveform and harmonic analysis: (a) before optimization; (b) after optimization.

and T_{avg} increases as much as possible. And the torque ripple does not increase.

In addition, h is chosen as the optimization variable A. l is chosen as the optimization variable B. And d is chosen as the optimization variable C. The initial values of the three optimization variables are (2, 6.5, 4). On this basis, appropriate values are selected as the level values. And optimization parameters and level values are shown in Table 2. Especially, "none" means no auxiliary slot.

3.3. Orthogonal Experimental Designs and Solution. The optimization goals, optimization variables, and corresponding level values have been determined above. The number of level values is not exactly the same. The traditional standard orthogonal experiment matrix cannot be established. According to principles of the Taguchi method experiment designing, the nonstandard orthogonal experimental matrix is established as shown in Table 3.

The rated operating point performance of each experiment can be calculated by using the two-dimensional finite element analysis method. The orthogonal experimental results are shown in Table 4. The calculation formula of THD is shown in formula (3). And the calculation of T_{avg} is shown in formula (5). T_{cog} can be obtained by the simulation analysis.

$$\mathrm{THD} = \frac{\sqrt{\sum_{i=2}^{n} x_i^2}}{x_1} \times 100\%, \tag{3}$$

$$T_{avg} = \frac{(T_{max} + T_{min})}{2}, \tag{4}$$

where x_1 is the effective value of the fundamental wave, x_i is the effective value of higher harmonics, and T_{max} and T_{min}

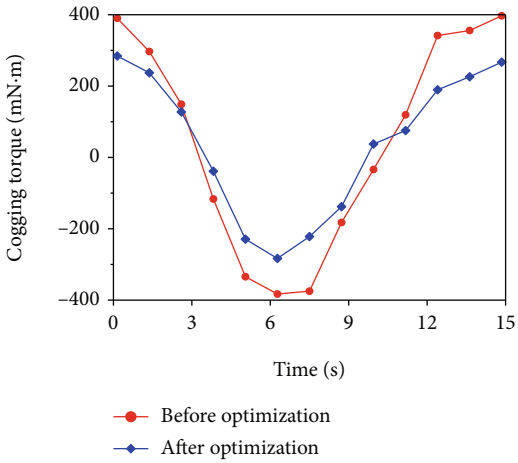

Figure 9: Cogging torque comparison.

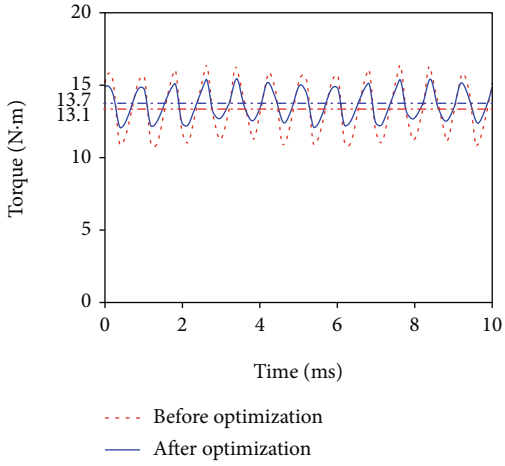

Figure 10: Output torque comparison.

are the maximum and minimum output torque, respectively. And they can be obtained by the simulation analysis.

3.4. Results Processing and Analysis. In the previous section, the results of each experiment were obtained by the two-dimensional finite element method. The overall average value of the experimental results can be calculated by formula (5). And the results are shown in Table 5.

$$\bar{m} = \frac{1}{18}\sum_{i=1}^{18} m_i. \quad (5)$$

The average value of each optimization variable can be calculated, respectively, at a certain level value. To give an example, the average value can be obtained by the following formula when the optimization variable A is selected as the level 1.

$$m_{A1}(\mathrm{THD}) = \frac{1}{3}(\mathrm{THD}(1) + \mathrm{THD}(7) + \mathrm{THD}(13)). \quad (6)$$

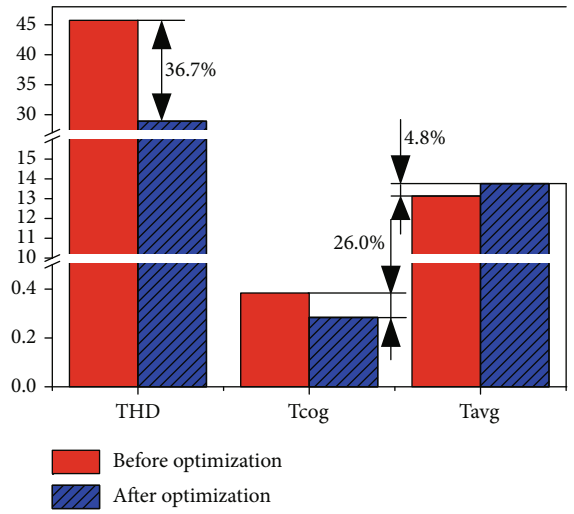

Figure 11: Performance comparison before and after optimization.

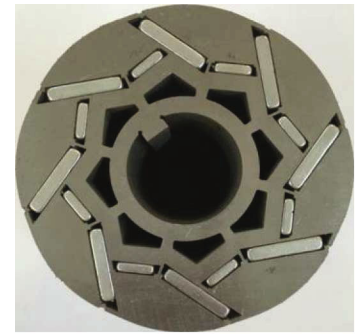

Figure 12: Rotor structure.

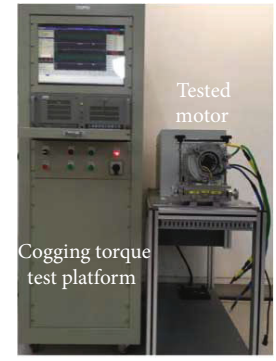

Figure 13: The cogging torque test platform.

Similarly, the average values of THD, T_{cog}, and T_{avg} can be obtained with reference to the calculation method of the above formula. And the results of THD, T_{cog}, and T_{avg} are shown in Table 6, Table 7, and Table 8, respectively.

If a single goal is optimized, the optimization combination can be selected in Table 6, Table 7, and Table 8. To optimize THD, a combination of A4, B1, and C2 can be selected. To optimize T_{cog}, a combination of A4, B2, and C3 can be selected. And a combination of A4, B3, and C3 can be selected to optimize T_{avg}.

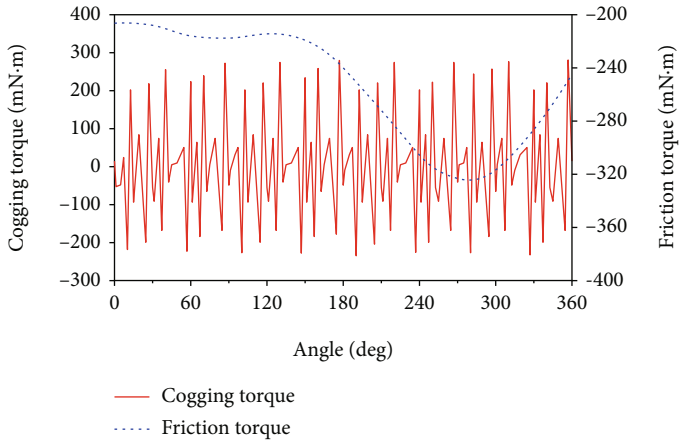

Figure 14: The cogging torque experimental curve.

It is necessary to analyze the influence of each optimization variable when multiobjective optimization is carried out. Based on the previous calculation, the proportions can be calculated by formula (7).

$$\mathrm{SS} = \frac{1}{x}\sum_{i=1}^{x}(m_x - \bar{m})^2, \tag{7}$$

where m_x is the value of each optimization goal under a certain level; $\bar{m}$ is the average value of each optimization goal; x is the number of levels, and SS is the variance of the optimization variable under a certain performance. And the calculation results are shown in Table 9.

In the above, the experimental results of the Taguchi method optimization are analyzed. And the proportions of the influence of each variable on the optimization goal are obtained. It can be seen that optimization variable A has a great influence on the three optimization goals. THD and T_{cog} are the smallest when level 4 is selected. And T_{avg} is the largest. Optimization variable B has a great influence on T_{cog}. Therefore, optimization variable B chooses level 2. And optimization variable C has a little influence on each optimization goal and chooses level 3. In other words, the eccentric distance is 8 mm. The length of the straight line is 6.5 mm. And the distance between auxiliary slots and a permanent magnet is 4.5 mm.

4. Simulation Analysis and Experimental Verification

4.1. Finite Element Simulation Analyses. According to the above optimization scheme, the motor structure after optimization is obtained and designed. The structure is shown in Figure 6. And the static magnetic field analysis is shown in Figure 7.

The optimized motor structure is analyzed by finite element simulation. The air-gap flux density waveform and harmonic analysis are compared and analyzed in Figure 8. The waveform after optimization meets an excepted waveform.

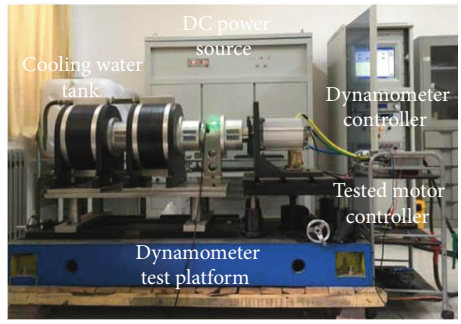

Figure 15: Dynamometer test platform.

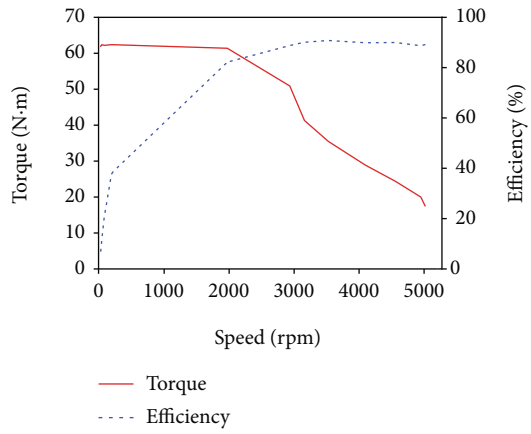

Figure 16: Motor characteristic curve.

Cogging torque comparison is shown in Figure 9. And output torque comparison is shown in Figure 10. With the two-dimensional finite element method simulation analysis, it can be calculated that THD is 28.9%. The T_{cog} is 284.3 mN•m. And the T_{avg} is 13.7 N•m.

It can be seen from Figure 10 that the T_{avg} is improved. And the range of the output torque ripple is reduced. The torque ripple rate (T_{ripple}) represents the torque ripple of the output torque. Its calculation is as follows:

$$T_{\text{ripple}} = \frac{T_{\max} - T_{\min}}{T_{\text{avg}}} \times 100\%. \quad (8)$$

It can be calculated that T_{ripple} before optimization is 41.1% by the above formula. And T_{ripple} after optimization is 24.7%. It decreases by 16.4%.

The performance comparison before and after optimization is shown in Figure 11. Compared with before optimization, THD is reduced by 36.7%. T_{cog} is reduced by 26.0%. And T_{avg} is increased by 4.8%.

4.2. Prototype Manufacture and Experiment. In order to verify the effectiveness of the simulation analysis, the rotor structure after optimization is manufactured. It is shown in Figure 12. The prototype is assembled and placed on a cogging torque test platform for experiment. The cogging torque test platform is shown in Figure 13.

The cogging torque experimental curve is shown in Figure 14. The maximum value is 280.8 mN•m. It is similar to the simulation value. Maximum friction torque is 346.8 mN•m.

In order to obtain the maximum torque and efficiency of asymmetrical magnetic pole PMSM, it is necessary to test the characteristic curve of the motor. The prototype is placed on the dynamometer test platform for a full load test. It is shown in Figure 15. And the characteristic curve of the motor is obtained as shown in Figure 16.

In Figure 16, the maximum speed of the motor is 5000 revolutions per minute. The maximum output torque is 62 N•m. And maximum efficiency exceeds 90%.

5. Conclusions

This paper proposes a novel asymmetric magnetic pole PMSM for automobiles. The equivalent magnetic circuit model is established. Many improvements have been made to the rotor structure. The Taguchi method is used to obtain the optimal solution of each optimization variable. Combined with finite element analysis and prototype experiment, the effectiveness of the structure and optimization method is verified. In addition, some conclusions are drawn as follows:

(1) The novel asymmetric magnetic pole permanent magnet synchronous motor has parallel effective magnetic flux. Compared with the traditional V-type structure, the total permeance is reduced. And the effective magnetic flux content is increased

(2) The Taguchi method is used to optimize the motor structure. A nonstandard orthogonal experimental matrix is established. The original 54 sets of experiments are replaced by 18 combinations of experiments. The number of experiments is reduced obviously. And the finite element method verifies the effectiveness of the method

(3) The eccentric distance of the rotor has the greatest influence on the total harmonic distortion of the air-gap flux density and the average output torque. The eccentric distance and the length of the straight line both have influence on the cogging torque. The proportions are approximately 50%

(4) Compared with the performance before optimization, the total harmonic distortion of the air-gap flux density reduced by 36.7%. The cogging torque is reduced by 26.0%. The average output torque is increased by 4.8%. And the output torque ripple is reduced by 16.4%

Data Availability

All data used to support the findings of this study are available from the corresponding author upon request.

Conflicts of Interest

The authors declare that there is no conflict of interest regarding the publication of this paper.

Acknowledgments

This research work is partially supported by the National Natural Science Foundation of China (Grant Nos. 51975340 and 51875327).

References

[1] W. Cao, B. C. Mecrow, G. J. Atkinson, J. W. Bennett, and D. J. Atkinson, "Overview of electric motor technologies used for more electric aircraft (MEA)," *IEEE Transactions on Industrial Electronics*, vol. 59, no. 9, pp. 3523–3531, 2011.

[2] Y. Guo, L. Shi, W. Zhang, C. Wenping, and K. Byung II, "Research on 3/6-phase winding switching integrated starter generator for range extender electric vehicles," *International Conference on Power Electronics and ECCE Asia*, pp. 2492–2497, 2019.

[3] R. Xu and C. Qin, "Development status and prospect of electric vehicle and its driving motor," *Southern Power System Technology*, vol. 10, no. 71, pp. 82–86, 2016.

[4] S. Ye, "Design and performance analysis of an iterative flux sliding-mode observer for the sensorless control of PMSM drives," *ISA Transactions*, vol. 94, pp. 255–264, 2019.

[5] K. Liu and J. Xu, "Life cycle evaluation of pure electric vehicle driving moto," *Acta Scientiae Circumstantiae.*, vol. 36, no. 9, pp. 3456–3463, 2016.

[6] X. Liu, H. Chen, J. Zhao, and A. Belahcen, "Research on the performances and parameters of interior PMSM used for electric vehicles," *IEEE Transactions on Industrial Electronics*, vol. 63, no. 6, pp. 3533–3545, 2016.

[7] W. Hu, X. Zhang, Y. Lei, Q. du, L. Shi, and G. Liu, "Analytical model of air-gap field in hybrid excitation and interior permanent magnet machine for electric logistics vehicles," *IEEE Access*, vol. 8, pp. 148237–148249, 2020.

[8] Q. Li, C. Sun, T. Fan, X. Wen, and Y. Li, "Rotor pole optimal design of double-layer interior permanent magnet machines for electric vehicle," *Electric Machines and Control*, vol. 24, no. 9, pp. 56–64, 2020.

[9] W. Ren, "A technique of torque ripple compensation for interior permanent magnet machines by using an asymmetrical V-

type rotor configuration," in *Annual Conference of the Industrial Electronics Society*, pp. 8744–8749, Beijing, China, 2017.

[10] Q. Chen, G. Xu, G. Liu, W. Zhao, L. Liu, and Z. Lin, "Torque ripple reduction in five-phase IPM motors by lowering interactional MMF," *IEEE Transactions on Industrial Electronics*, vol. 65, no. 11, pp. 8520–8531, 2018.

[11] W. Ren, Q. Xu, Q. Li, and L. Zhou, "Reduction of cogging torque and torque ripple in interior PM machines with asymmetrical V-type rotor design," *IEEE Transactions on Magnetics*, vol. 52, no. 7, pp. 1–5, 2016.

[12] F. Chai, P. Liang, Y. Pei, and S. Cheng, "Magnet shape optimization of surface-mounted permanent-magnet motors to reduce harmonic iron losses," *IEEE Transactions on Magnetics*, vol. 52, no. 7, pp. 1–4, 2016.

[13] J. He, G. LI, R. Zhou, and Q. Wang, "Optimization of permanent-magnet spherical motor based on Taguchi method," *IEEE Transactions on Magnetics*, vol. 52, no. 2, pp. 1–7, 2020.

[14] C. Xia, L. Guo, Z. Zhang, T. Shi, and H. Wang, "Optimal designing of permanent magnet cavity to reduce iron loss of interior permanent magnet machine," *IEEE Transactions on Magnetics*, vol. 51, no. 12, pp. 1–9, 2015.